

THE MOST METAL-POOR STARS. III. THE METALLICITY DISTRIBUTION FUNCTION AND CEMP FRACTION^{1,2,3}

DAVID YONG⁴, JOHN E. NORRIS⁴, M. S. BESSELL⁴, N. CHRISTLIEB⁵, M. ASPLUND^{4,6}, TIMOTHY C. BEERS^{7,8}, P. S. BARKLEM⁹, ANNA FREBEL¹⁰, AND S. G. RYAN¹¹

Draft version August 16, 2012

ABSTRACT

We examine the metallicity distribution function (MDF) and fraction of carbon-enhanced metal-poor (CEMP) stars in a sample that includes 86 stars with $[\text{Fe}/\text{H}] \leq -3.0$, based on high-resolution, high-S/N spectroscopy, of which some 32 objects lie below $[\text{Fe}/\text{H}] = -3.5$. After accounting for the completeness function, the “corrected” MDF does not exhibit the sudden drop at $[\text{Fe}/\text{H}] = -3.6$ that was found in recent samples of dwarfs and giants from the Hamburg/ESO survey. Rather, the MDF decreases smoothly down to $[\text{Fe}/\text{H}] = -4.1$. Similar results are obtained from the “raw” MDF. We find the fraction of CEMP objects below $[\text{Fe}/\text{H}] = -3.0$ is $23 \pm 6\%$ and $32 \pm 8\%$ when adopting the Beers & Christlieb and Aoki et al. CEMP definitions, respectively. The former value is in fair agreement with some previous measurements, which adopt the Beers & Christlieb criterion.

Subject headings: Cosmology: Early Universe, Galaxy: Formation, Galaxy: Halo, Nucleosynthesis, Abundances, Stars: Abundances

1. INTRODUCTION

Metal-poor stars provide critical information on the earliest phases of Galactic formation (see e.g., the reviews by Beers & Christlieb 2005 and Frebel & Norris 2011). Their chemical abundances shed light upon the nature of the first stars to have formed in the Universe, and the nucleosynthesis which seeded all subsequent generations of stars.

This is the third paper in our series, which focuses upon the discovery of, and high-resolution, high signal-to-noise ratio (S/N) spectroscopic analysis of, the most metal-poor stars. Here we explore two key issues: the metallicity distribution function (MDF) and the fraction of carbon-enhanced metal-poor (CEMP)¹² stars at lowest metallicities.

Any model purporting to explain the formation and evolution of our Galaxy must be able to reproduce the observed MDF. The ingredients of such models include the initial mass function (IMF), nucleosynthetic yields, and inflow or outflow of gas. Observations of the MDF can constrain these initial conditions and physical processes. Since the early work by Hartwick (1976), measurements of the MDF involve increasing numbers of stars with more accurate metallicity measurements (see e.g., Laird et al. 1988; Ryan & Norris 1991). One of the basic predictions of Hartwick’s Simple Model of Galactic Chemical Enrichment is that the number of stars having abundance less than a given metallicity should decrease by a factor of ten for each factor of ten decrease in metallicity¹³. Norris (1999) presented observational support for this suggestion, down to $[\text{Fe}/\text{H}] \sim -4.0$, below which it appeared to be no longer valid. More recently, Schörck et al. (2009) and Li et al. (2010) presented MDFs of the Galactic halo using 1638 giant and 617 dwarf stars, respectively, from the Hamburg/ESO Survey (HES; Wisotzki et al. 1996). Below $[\text{Fe}/\text{H}] = -2.5$, the MDFs for dwarfs and giants were in excellent agreement. A prominent feature of both MDFs was the apparent lack of stars more metal-poor than $[\text{Fe}/\text{H}] = -3.6$. While a handful of such stars are known, the sharp cutoff in the MDF has important implications for the critical metallicity above which low-mass star formation is possible (e.g., Salvadori et al. 2007). More detailed studies of the MDF, and in particular the low-metallicity tail, are necessary to confirm and constrain the star formation modes of the first stars (e.g., Bromm & Larson 2004).

The HK survey (Beers et al. 1985, 1992) revealed that there is a large fraction of metal-poor stars with unusually strong CH G-bands indicating high C abundances. With the addition of numerous metal-poor stars found in the HES, the CEMP fraction at low metallicity has been confirmed and quantified, with estimates ranging from 9% (Frebel et al. 2006) to > 21% (Lucatello et al. 2006). These numbers are consid-

(Beers & Christlieb 2005).

¹³ While a number of chemical evolution models (e.g., Kobayashi et al. 2006, Karlsson 2006, Salvadori et al. 2007, Prantzos 2008, and Cescutti & Chiappini 2010) have improved upon the one-zone closed-box Hartwick model, the general behavior remains largely unchanged.

¹ This paper includes data gathered with the 6.5 meter Magellan Telescopes located at Las Campanas Observatory, Chile.

² Some of the data presented herein were obtained at the W. M. Keck Observatory, which is operated as a scientific partnership among the California Institute of Technology, the University of California and the National Aeronautics and Space Administration. The Observatory was made possible by the generous financial support of the W. M. Keck Foundation.

³ Based on observations collected at the European Organisation for Astronomical Research in the Southern Hemisphere, Chile (proposal 281.D-5015).

⁴ Research School of Astronomy and Astrophysics, The Australian National University, Weston, ACT 2611, Australia; yong@mso.anu.edu.au, jen@mso.anu.edu.au, bessel@mso.anu.edu.au, martin@mso.anu.edu.au

⁵ Zentrum für Astronomie der Universität Heidelberg, Landessternwarte, Königstuhl 12, D-69117 Heidelberg, Germany; n.christlieb@lsw.uni-heidelberg.de

⁶ Max-Planck Institute for Astrophysics, Karl-Schwarzschild Str. 1, 85741, Garching, Germany

⁷ National Optical Astronomy Observatory, Tucson, AZ 85719

⁸ Department of Physics & Astronomy and JINA: Joint Institute for Nuclear Astrophysics, Michigan State University, E. Lansing, MI 48824, USA; beers@pa.msu.edu

⁹ Department of Physics and Astronomy, Uppsala University, Box 515, 75120 Uppsala, Sweden; paul.barklem@physics.uu.se

¹⁰ Massachusetts Institute of Technology, Kavli Institute for Astrophysics and Space Research, Cambridge, MA 02139, USA; afrebel@mit.edu

¹¹ Centre for Astrophysics Research, School of Physics, Astronomy & Mathematics, University of Hertfordshire, College Lane, Hatfield, Hertfordshire, AL10 9AB, UK; s.g.ryan@herts.ac.uk

¹² Initially defined as stars with $[\text{C}/\text{Fe}] \geq +1.0$ and $[\text{Fe}/\text{H}] \leq -2.0$

erably larger than the fraction of C-rich objects at higher metallicity, the so-called CH and Ba stars, which account for only $\sim 1\%$ of the population. The fraction is even larger at lowest metallicity: below $[\text{Fe}/\text{H}] < -4.5$, 75% of the four known stars belong to the CEMP class (Norris et al. 2007; Caffau et al. 2011). To explain these large fractions, several studies argue that adjustments to the IMF are necessary (e.g., Lucatello et al. 2005; Komiya et al. 2007; Izzard et al. 2009). Carollo et al. (2012) offer an alternative interpretation for the increase of the CEMP fraction they observe in the range $-3.0 < [\text{Fe}/\text{H}] < -1.5$ in terms of a dependence of CEMP fraction on height above the Galactic plane. In their most metal-poor bin at $[\text{Fe}/\text{H}] \sim -2.7$, they report C-rich fractions of 20% and 30% for their inner- and outer-halo components, respectively (see their Figure 15). In their view, this can be accounted for by the presence of different carbon-production mechanisms (some not involving the presence of AGB nucleosynthesis) that have operated in the inner- and outer-halo populations.

An understanding of the CEMP stars is complicated by the fact that they do not form a homogeneous group: Beers & Christlieb (2005) define several CEMP subclasses (all of which have $[\text{C}/\text{Fe}] > +1.0$) as follows: (i) CEMP-r – $[\text{Eu}/\text{Fe}] > +1.0$; (ii) CEMP-s – $[\text{Ba}/\text{Fe}] > +1.0$ and $[\text{Ba}/\text{Eu}] > +0.5$; (iii) CEMP r/s – $0.0 < [\text{Ba}/\text{Eu}] < +0.5$; and CEMP-no – $[\text{Ba}/\text{Fe}] < 0.0$. Aoki (2010) shows that below $[\text{Fe}/\text{H}] = -3.0$, the CEMP stars are principally (90%) CEMP-no stars, while for $[\text{Fe}/\text{H}] > -3.0$, the CEMP-s class predominates. These differences lie outside the scope of the present paper. Here we seek to constrain only the fraction of CEMP stars at lowest abundance, $[\text{Fe}/\text{H}] < -3.0$, and to compare the results with the fractions determined at higher abundances. In Paper IV (Norris et al. 2012b) we shall address the nature of the CEMP-no stars, which comprise the large majority of CEMP stars in our extremely metal-poor sample.

2. OBSERVATIONS AND ANALYSIS

In Norris et al. (2012a; Paper I), we presented high-resolution spectroscopic observations of 38 extremely metal-poor stars ($[\text{Fe}/\text{H}] < -3.0$; 34 newly discovered), obtained using the Keck, Magellan, and VLT telescopes, including the discovery and sample selection, equivalent-width measurements, radial velocities, and line list. In Paper I, we also described the temperature scale, which consists of spectrophotometry and Balmer-line analysis. In addition to the 38 program stars, we selected 207 stars from the SAGA database (Suda et al. 2008) (queried on 2 Feb 2010), and performed a homogeneous re-analysis of this literature sample. All stars were analyzed using the NEWODF grid of ATLAS9 model atmospheres (Castelli & Kurucz 2003), and the 2011 version of the stellar line-analysis program MOOG (Sneden 1973), which includes proper treatment of continuum scattering (Sobeck et al. 2011). They thus have effective temperatures, surface gravities, microturbulent velocities, $\log g_f$ values, solar abundances (Asplund et al. 2009), and therefore metallicities, $[\text{Fe}/\text{H}]$, all on the same scale.

The literature sample was reduced from 207 to 152 stars by (i) discarding stars with fewer than 14 Fe I lines (the minimum number of Fe I lines measured in our program stars), (ii) removing literature stars included in the program-star sample, and (iii) averaging the results of stars having multiple analyses into a single set of abundances. Thus, the final combined sample consists of 190 stars (38 program stars and 152 literature stars). Full details regarding the analysis are presented in Yong et al. (2012, Paper II).

3. RESULTS

3.1. Selection Biases

In Table 1, we present data, based on our high-resolution analyses, for the 86¹⁴ stars in our collective sample that have $[\text{Fe}/\text{H}] \leq -3.0$; of these, 32 have $[\text{Fe}/\text{H}] \leq -3.5$, while there are nine with $[\text{Fe}/\text{H}] \leq -4.0$. We stress again that these metallicities are on our homogeneous system of T_{eff} , $\log g$, ξ_t , $\log g_f$ values, and solar abundances. These are the most metal-poor stars known in our Galaxy, and allow us to address below the key issues of the MDF and CEMP fraction.

Before continuing, we comment on the completeness function and selection biases of the sample. The HES is complete for metallicities below $[\text{Fe}/\text{H}] = -3.0$ (Schörck et al. 2009; Li et al. 2010). To estimate the completeness, Schörck et al. (2009) and Li et al. (2010) used the Simple Model to generate a metallicity distribution function and then applied their selection criteria to obtain the MDF which would have been observed in the HES (see Section 6 in Schörck et al. 2009, and Section 3.4 in Li et al. 2010 for further details). From Paper I, we can compute the completeness function for the ~ 30 HES candidates having high-resolution, high-S/N spectra discovered in that work. First, we use a linear transformation to place the medium-resolution metallicities, $[\text{Fe}/\text{H}]_{\text{K}}$, from Paper I onto the high-resolution abundance scale, $[\text{Fe}/\text{H}]$. We then compare the number of HES stars observed at high resolution with the total number of HES stars observed at medium resolution, and from which the stars observed at high resolution were selected, as a function of $[\text{Fe}/\text{H}]$. We use this ratio to correct the MDFs in the following subsection. In a similar manner, we are able to determine the completeness function for the ~ 50 HK-survey stars in our extended sample, by using material in the medium-resolution HK database maintained by T. C. B.

3.2. The Metallicity Distribution Function (MDF)

Our MDFs are presented in Figure 1¹⁵, where in the left panels the scale of the ordinate is linear and for those on the right it is logarithmic. The two uppermost panels each contain MDFs constructed from the raw data for the 38 program stars and the total sample of 190 objects. We use generalized histograms, in which each data point is replaced by a Gaussian of width $\sigma = 0.30$ ¹⁶ dex. The Gaussians are then summed to produce a realistically smoothed histogram.

Construction of our smoothed MDF includes uncertainties, which we estimate in the following manner using Monte Carlo simulations. We replaced each data point, $[\text{Fe}/\text{H}]$, with a random number drawn from a normal distribution of width 0.15 dex, centered at the $[\text{Fe}/\text{H}]$ of the given data point. We repeated this process for each data point in our collective sample of 190 stars, and a generalized histogram was constructed

¹⁴ For nine program stars, we could not determine whether they were dwarfs or subgiants. For the subset of those stars included in this paper, we present the results for both cases in Table 1. In all figures, unless noted otherwise, we adopt the average $[\text{Fe}/\text{H}]$ and $[\text{X}/\text{Fe}]$ from the dwarf and subgiant analyses for these stars. For the nine objects, the average differences are $\langle [\text{Fe}/\text{H}]_{\text{dwarf}} - [\text{Fe}/\text{H}]_{\text{subgiant}} \rangle = 0.02 \pm 0.01$ dex ($\sigma = 0.03$) and $\langle [\text{X}/\text{Fe}]_{\text{dwarf}} - [\text{X}/\text{Fe}]_{\text{subgiant}} \rangle = 0.05 \pm 0.02$ dex ($\sigma = 0.17$), where X refers to the 14 species (from Na to Ba) measured in Paper II. For C, while the differences are larger, $\langle [\text{C}/\text{Fe}]_{\text{subgiant}} - [\text{C}/\text{Fe}]_{\text{dwarf}} \rangle = 0.23 \pm 0.05$ dex ($\sigma = 0.13$), the CEMP classifications do not depend on whether we adopt the dwarf or subgiant value.

¹⁵ All figures were generated using the full sample, presented in Paper II.

¹⁶ We regard our typical uncertainty in $[\text{Fe}/\text{H}]$ to be 0.15 dex, rather than 0.30 dex. Given our still relatively limited sample size, using $\sigma = 0.15$ dex produces spurious structure in our MDF. None of our conclusions depend upon our choice of σ in constructing the MDF.

TABLE 1
STELLAR PARAMETERS AND CARBON ABUNDANCE

Star	RA2000 ^a	DEC2000 ^a	T_{eff} (K)	$\log g$ (cgs)	ξ_r (km s ⁻¹)	[M/H] _{model}	[Fe/H] _{derived}	[C/Fe] ^b	C-rich ^c	Source
(1)	(2)	(3)	(4)	(5)	(6)	(7)	(8)	(9)	(10)	(11)
CS29527-015	00 29 10.7	-19 10 07.2	6577	3.89	1.9	-3.3	-3.32	1.18	1	5
CS30339-069	00 30 16.0	-35 56 51.2	6326	3.79	1.4	-3.1	-3.05	0.56	0	5
CS29497-034	00 41 39.8	-26 18 54.4	4983	1.96	2.0	-3.0	-3.00	2.72	1	4
HD4306	00 45 27.2	-09 32 39.9	4854	1.61	1.6	-3.1	-3.04	0.11	0	12
CD-38 245	00 46 36.2	-37 39 33.5	4857	1.54	2.2	-4.2	-4.15	< -0.33	0	7
HE0049-3948	00 52 13.4	-39 32 36.9	6466	3.78	0.8	-3.7	-3.68	< 1.81	0	1
HE0057-5959	00 59 54.0	-59 43 29.9	5257	2.65	1.5	-4.1	-4.08	0.86	1	1
HE0102-1213	01 05 28.0	-11 57 31.1	6100	3.65	1.5	-3.3	-3.28	< 1.31	0	1
CS22183-031	01 09 05.1	-04 43 21.1	5202	2.54	1.1	-3.2	-3.17	0.42	0	12
HE0107-5240	01 09 29.2	-52 24 34.2	5100	2.20	2.2	-5.3	-5.54	3.85	1	8

REFERENCES. — 1 = This study; 2 = Aoki et al. (2002); 3 = Aoki et al. (2006); 4 = Aoki et al. (2007); 5 = Bonifacio et al. (2007, 2009); 6 = Carretta et al. (2002); Cohen et al. (2002); 7 = Cayrel et al. (2004); Spite et al. (2005); 8 = Christlieb et al. (2004); 9 = Cohen et al. (2006); 10 = Cohen et al. (2008); 11 = Frebel et al. (2007b); 12 = Honda et al. (2004); 13 = Lai et al. (2008); 14 = Norris et al. (2001); 15 = Norris et al. (2007)

Note. Table 1 is published in its entirety in the electronic edition of The Astrophysical Journal. A portion is shown here for guidance regarding its form and content.

^a Coordinates are on the 2MASS system (Skrutskie et al. 2006)

^b For literature stars, [C/Fe] is the (average) value from the reference(s).

^c We adopt the Aoki et al. (2007) CEMP definition.

^d This analysis assumes the star is a dwarf.

^e This analysis assumes the star is a subgiant.

for this new sample. We repeated this process for 10,000 new random samples, producing a generalized histogram for each new random sample. At a given [Fe/H], we then have a distribution of some 10,000 values, one for each MDF. We measured the FWHM of this distribution, and adopt this value as an estimate of the uncertainty in our MDF at a given [Fe/H]. In Figure 1(c), we plot the fractional uncertainty, where a value of 0.2 represents a 20% uncertainty in the value of the MDF. The relative uncertainty reaches 50% near [Fe/H] = -4.2, and becomes rapidly larger at lower metallicities, indicating that the sample size loses much statistical significance below this value.

We also constructed a regular histogram to compare with the smoothed MDF. We employed the Shimazaki & Shinomoto (2007) algorithm to determine the optimal bin width (0.272 dex) for the full 190 star sample. As expected, both histograms exhibit a similar behavior.

We corrected the “program star MDF” using the HES completeness function described above in Section 3.1 (here shown together with the HK completeness function in Figure 1(d)), leaving the “literature sample MDF” unchanged. These MDFs are presented in Figure 1 (panels e-f). We also corrected the full MDF (i.e., “program star + literature sample” MDF) using the HES completeness function, and plot both corrected MDFs in Figure 1 (panels g-h). While the selection biases associated with the discovery of the stars in the SAGA database are not explicit, almost half of the 86 stars (42) in Table 1 carry HK-survey names, while most others (36) have HES-survey nomenclature. It is clear that the majority of stars in Table 1 have been found in those low-resolution spectroscopic surveys, and thus inherit the spectroscopic- and volume-selection biases of those works, plus additional biases imposed in later follow-up with medium- and high-resolution spectroscopy. Many of the HK-survey stars would also have been recovered in the HES survey, but were not renamed. Consequently, using the HES completeness function should be a reasonable step. Given the clear similarity between the HES and HK completeness functions below [Fe/H] = -3.3, the corrected MDF would be essentially identical in this

metallicity regime had we used the HK completeness function.

We use a two-sample Kolmogorov-Smirnov (KS) test to compare the MDFs for dwarfs ($\log g > 3.5$) and giants ($\log g < 3.5$). The null hypothesis is that the dwarf and giant MDFs are drawn from the same distribution. For [Fe/H] \leq -3.0, the two-sample KS test yields a probability of 0.601 ($D = 0.167$) that the dwarf and giant MDFs are drawn from the same distribution¹⁷. A similar test for [Fe/H] \leq -3.5 yields a probability of 0.915 ($D = 0.200$) that the dwarf and giant MDFs are drawn from the same distribution. Therefore, the null hypothesis that the giants and dwarfs are drawn from the same population cannot be rejected at the 0.10 level of significance, the least stringent level in Table M of Siegel (1956).

In Figure 1(a), we overplot the raw MDF from Schörck et al. (2009) (using the values in their Table 3). Comparing our sample with Schörck et al. (2009) and Li et al. (2010) (made available by N. C.), we find 12 stars in common. For these 12 stars, there are some 18 [Fe/H] measurements that can be compared. For the nine program stars for which we conducted dwarf and subgiant analyses, we treat both [Fe/H] values as independent measurements for the purposes of this comparison. Our metallicities differ from the Schörck et al. (2009) and Li et al. (2010) values by -0.26 ± 0.06 dex ($\sigma = 0.27$ dex), and so we shift the raw HES MDF of Schörck et al. (2009) by -0.26 dex in Figure 1, and scale it to match our MDF at [Fe/H] = -3.5. Below [Fe/H] = -3.5, we find a large fraction of stars relative to the HES MDF. In Figure 1(f), both the program star and literature sample MDFs have a slope close to 1.0, consistent with the Hartwick Simple Model, down to the shoulder at [Fe/H] \simeq -4.1, when the finite sample begins to run out of stars (which are necessarily counted in integers). This corresponds to the metallicity at which the fractional error (Figure 1(c)) increases rapidly and, as noted above, the finite sample size loses much statistical significance.

Therefore, taken at face value, and bearing in mind the bi-

¹⁷ The dwarf and giant MDFs for [Fe/H] \leq -3.0 may be seen in Figure 6 panels (d) and (e), respectively, which we shall discuss in what follows.

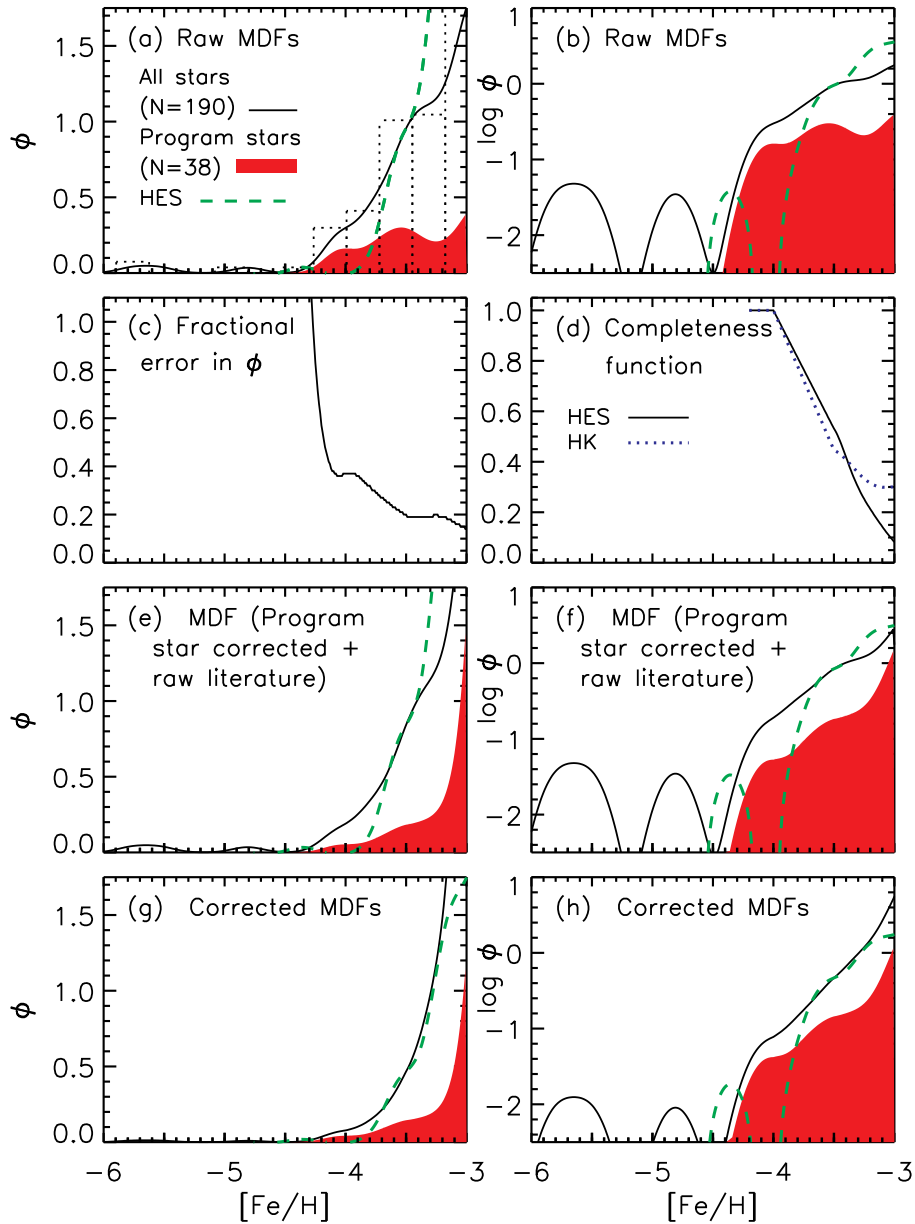


FIG. 1.— Generalized histograms showing the MDF (linear (left) and logarithmic (right) scales). The full sample (solid black line) and program stars (red histogram) are shown. The green dashed line is the raw HES MDF from Schörck et al. (2009), shifted by -0.29 dex and scaled to match our MDF at $[\text{Fe}/\text{H}] = -3.5$. Panel (a) includes a regular histogram (dotted line) employing the Shimazaki & Shinomoto (2007) optimal bin width algorithm. Panel (c) shows the fractional uncertainty in our MDF (e.g., a fractional uncertainty of 0.2 represents an error of 20% of the MDF value.) Panel (d) shows the HES and HK completeness functions. The HES completeness function is applied to the MDFs shown in panels (e,f,g,h).

ases, the apparent cutoff in the HES MDF at $[\text{Fe}/\text{H}] = -3.6$ is not confirmed by our data. We identify 13 HES stars in our sample that have $[\text{Fe}/\text{H}] \leq -3.7$ (of which four are contained in the work of Schörck et al. 2009 and Li et al. 2010). We speculate that (i) stars in our sample having $[\text{Fe}/\text{H}] < -3.7$ were rejected as having strong G -bands ($\text{GP}^{18} > 6 \text{ \AA}$), and/or (ii) our abundance scale differs from that adopted in the Schörck et al. (2009) and Li et al. (2010) analyses.

Regarding point (i), none of our objects has $\text{GP} > 6 \text{ \AA}$. In particular, we note that the three most Fe-poor HES stars, all of which have large $[\text{C}/\text{Fe}]$ ratios, are not rejected by this criterion. Concerning point (ii), Figure 2 shows the metallic-

ity difference $\Delta[\text{Fe}/\text{H}] = [\text{Fe}/\text{H}]$ (high resolution: this study) $- [\text{Fe}/\text{H}]_{\text{K}}$ (medium resolution: Schörck et al. 2009; Li et al. 2010) versus T_{eff} , $\log g$, $[\text{Fe}/\text{H}]$, $E(B-V)$, and GP. In each panel, we plot the linear least squares fit to the data, and show the formal slope and uncertainty as well as the dispersion about the slope. In all cases, the dispersion about the slope is compatible with the value expected based on the convolution of the errors, σ (combined) = 0.25 dex assuming σ (this study) = 0.15 dex and σ (Beers et al. 1999) = 0.20 dex. The correlation between $\Delta[\text{Fe}/\text{H}]$ versus $[\text{Fe}/\text{H}]$ is significant at the $2\text{-}\sigma$ level (although we caution that the errors on these two quantities are correlated), indicating that as one moves to lower metallicity, the $[\text{Fe}/\text{H}]$ values from our high-resolution analysis are lower than those based on medium-resolution spectra. Such a correlation would help, in part, to explain why

¹⁸ This is the Beers et al. (1999) index that measures the strength of the 4300Å CH molecular features.

we do not find a cutoff in the MDF. Possible explanations for this correlation include systematic differences in the analyses, interstellar Ca absorption lines, and/or CH molecular stellar lines in the region of the Ca II K line. Further insight into the differences from high-resolution and medium-resolution spectra await larger comparison samples. (We also note that Figure 2 includes 3- σ correlations between $\Delta[\text{Fe}/\text{H}]$ and T_{eff} (panel a) and $\Delta[\text{Fe}/\text{H}]$ and $\log g$ (panel b).) For completeness, we note that linear regression analysis shows that the best fit to $\Delta[\text{Fe}/\text{H}]$ (high resolution – medium resolution) is $-1.825 + 2.442 \times 10^{-4} \times T_{\text{eff}} + 0.151 \times \log g + 0.160 \times [\text{Fe}/\text{H}]_{\text{high resolution}} - 0.401 \times E(B-V) + 0.337 \times \text{GP}$. The dispersion about this fit is 0.17 dex, and the uncertainties in the coefficients are 2.986×10^{-4} , 0.147, 0.189, 6.637, and 0.295 for T_{eff} , $\log g$, $[\text{Fe}/\text{H}]$, $E(B-V)$, and GP, respectively.

In Figure 3, we compare the raw and corrected MDFs with several model predictions, scaled to match our MDFs at $[\text{Fe}/\text{H}] = -3.5$. The rationale for choosing this normalization is that (i) in this metallicity regime we expect that our sample includes the vast majority of stars currently known, albeit with selection biases, and (ii) we hope to provide a more detailed consideration of the MDF at the lowest observed $[\text{Fe}/\text{H}]$ values.

All predictions, except the Kobayashi et al. (2006) “outflow” model, provide a reasonable fit to the raw and corrected MDFs. The Kobayashi et al. (2006) “infall” model provides a superior fit to our MDF than their “outflow” model (which overpredicts the number of metal-poor stars). The “outflow” model contains (i) outflow, (ii) no infall, and (iii) a low star-formation efficiency, while the “infall” model contains (i) no outflow, (ii) infall, and (iii) a much lower star-formation efficiency. Prantzos (2008) adopts a hierarchical merging framework in which the halo is formed from sub-halos, with a distribution in stellar mass, and with the MDF of each sub-halo based on Local Group dwarf satellite galaxies. Both Prantzos models (“outflow” only and “outflow+infall”) provide equally good fits to our MDF. Salvadori et al. (2007) provide predictions for different critical metallicities, Z_{cr} , and their $Z_{\text{cr}} = 10^{-4} Z_{\odot}$ and $Z_{\text{cr}} = 0$ models both provide reasonable fits to our MDF. The raw and corrected MDFs indicate that the critical metallicity, above which low-mass star formation is possible, is well below $Z_{\text{cr}} = 10^{-3.4} Z_{\odot}$, in contrast to the Schörck et al. (2009) and Li et al. (2010) MDFs. In addition to the spectroscopic selection biases noted earlier, we need to be mindful of possible volume-selection biases, and that the real Galactic MDF at low metallicities could be significantly different from the one presented in this paper. Still larger, deeper samples, the biases and completeness of which are better understood, are necessary to obtain this MDF.

3.2.1. On the nature of the MDF

We now explore four aspects of our MDF analysis: (1) choice of a lower-metallicity cutoff versus a higher-metallicity cutoff, (2) usage of a regular histogram versus a generalized histogram, (3) adoption of a linear versus a logarithmic scale, and (4) inclusion of elements in addition to Fe when defining the metallicity.

Lower-metallicity cutoff versus higher-metallicity cutoff

In order to explore the first aspect, we adopt the (one-zone, closed-box) Simple Model of Galactic chemical evolution (Schmidt 1963; Searle & Sargent 1972; Pagel & Patchett

1975; Hartwick 1976), and create two MDFs, from which we remove all stars below $[\text{Fe}/\text{H}] = -4.5$ (lower-metallicity cutoff) and -4.0 (higher-metallicity cutoff, sometimes referred to as a “sharp cutoff”). Both are populated with stars on a regular grid of step size 0.05 dex, and normalized such that they have 1000 stars below $[\text{Fe}/\text{H}] = -3.0$, i.e., some 12 times larger than our 86 star sample in Table 1. For the lower-metallicity cutoff (MDF1), there are four stars in the lowest metallicity bin, $[\text{Fe}/\text{H}] = -4.5$, while for the higher-metallicity cutoff (MDF2), there are 20 stars in the lowest metallicity bin, $[\text{Fe}/\text{H}] = -4.0$. The two MDFs are shown in Figure 4. In the upper panel, one sees that when overplotted on the full metallicity range, $-5.0 < [\text{Fe}/\text{H}] < 0.0$, they are indistinguishable. When considering only the regime below $[\text{Fe}/\text{H}] = -3.0$ (Figure 4 panels (b) and (c)), however, the difference in the two MDFs is clear.

Regular histogram versus generalized histogram

Panels (b) and (c) of Figure 4 show regular histograms for the two MDFs, while panels (f) and (g) show generalized histograms. As expected, the generalized histogram smooths out the data along the abscissa. Given the numbers of stars in the lowest metallicity bins, the lower-metallicity cutoff MDF may appear to have an “extended tail,” when represented in generalized histogram format, but in reality, both MDFs now have an additional tail.

Linear versus logarithmic scale

Panels (b,c,f,g) and (d,e,h,i) of Figure 4 have linear and logarithmic scales respectively. Panels (d) and (e) (regular histograms) and panels (h) and (i) (generalized histograms) exhibit rather similar trends. When using a logarithmic scale, it is easier to discern where the MDF cuts off, (as every finite sample, observed or simulated, must). The generalized histogram replaces each datum with a Gaussian function, and taking the logarithm of this yields an inverted quadratic function; i.e., each datum contributes an inverted quadratic function to the log panel. In Figure 4(h), the last Monte Carlo datum at $[\text{Fe}/\text{H}] = -4.5$ gives rise to the quadratic roll-off at $[\text{Fe}/\text{H}] < -4.5$, and in Figure 4(i) the last Monte Carlo datum at $[\text{Fe}/\text{H}] = -4.0$ gives rise to the roll-off at $[\text{Fe}/\text{H}] < -4.0$. This roll-off meets the populated part of the MDF at a “shoulder”, above which the MDF rises with a slope of 1.0, due to the adoption of the Simple Model. The location of the shoulder indicates the metallicity at which either the finite sample size becomes too small to populate the MDF, as in this simulation, or the MDF genuinely departs from the Galactic chemical evolution model pertaining at higher metallicity, as would be the case in the scenarios envisaged by Salvadori et al. (2007) and others discussed in connection with Figure 3. The fact that the shoulder in our observed MDF (e.g., Figures 1(f), 1(h) or Figure 3), determined from high-resolution spectroscopic analyses, is located at $[\text{Fe}/\text{H}] = -4.1$ or -4.2 , and attains a slope close to 1.0 at higher metallicity, gives us the confidence that the MDF does not exhibit a sharp drop at $[\text{Fe}/\text{H}] = -3.6$, nor indeed in the metallicity range down to $[\text{Fe}/\text{H}] = -4.1$.

Inclusion of elements in addition to Fe in the “metallicity”

Strictly defined, metallicity (Z) includes all elements heavier than helium, although in practice Fe is widely adopted as the canonical measure of stellar metallicity. Therefore, the

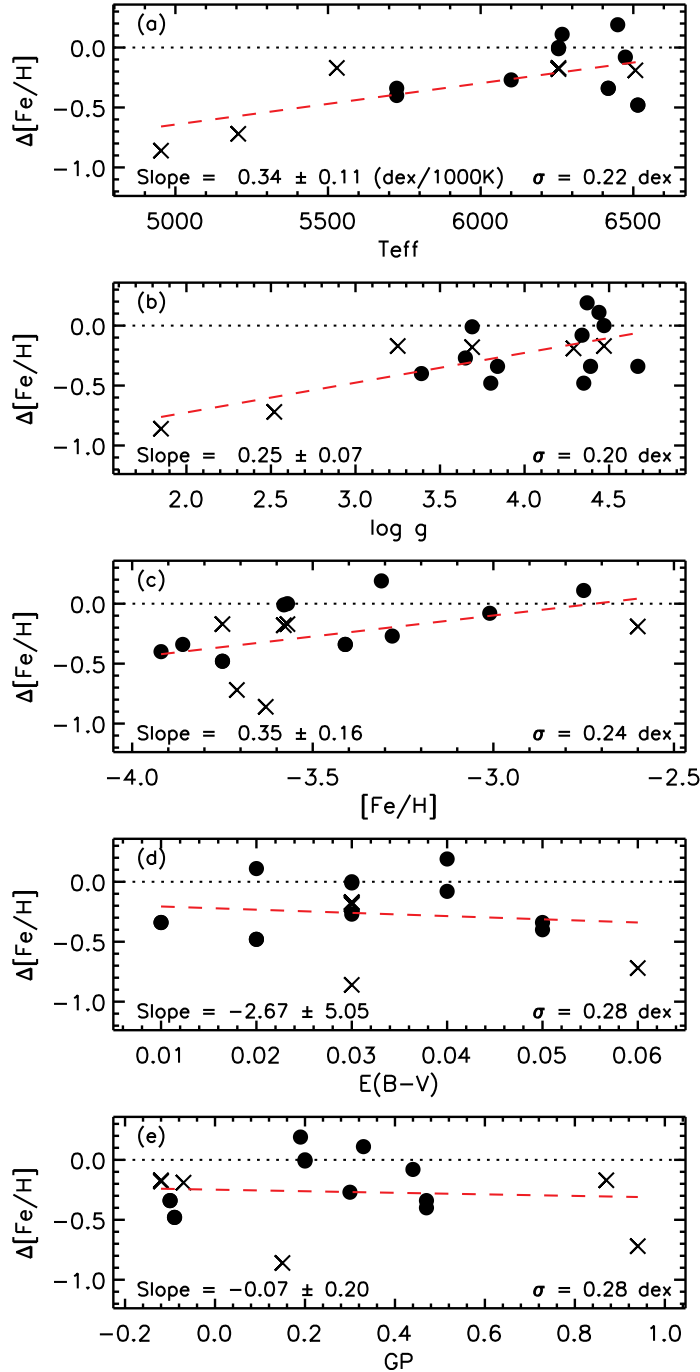


FIG. 2.— The difference in metallicity (This Study – Literature) between our analysis and those of Schörck et al. (2009) (crosses) and Li et al. (2010) (circles) vs. (a) T_{eff} , (b) $\log g$, (c) $[\text{Fe}/\text{H}]$, (d) $E(B-V)$, and (e) GP, where the abscissa values in panels (a), (b), and (c) were obtained from the high-resolution analysis. In each panel, we plot the linear least squares fit to the data, and show the slope, uncertainty, and dispersion about the slope. In this figure, we include both the dwarf and subgiant $[\text{Fe}/\text{H}]$ measurements for those program stars with multiple analyses (see Section 2 for details).

MDF discussed thus far is really the Fe distribution function. For the Sun, the seven most abundant metals, in decreasing order, are O, C, Ne, N, Mg, Si, and Fe (Asplund et al. 2009). Therefore, in order to explore this fourth aspect of our discussion, the behavior of the MDF when including additional elements, we arbitrarily define Z to consist of C, N, Mg, Si, and Fe. (Of the 86 stars with $[\text{Fe}/\text{H}] \leq -3.0$, there are measurements of C, N, Mg, and Si for 54, 36, 81, and 36 stars respectively.) We compute Z for each star, only considering the set of elements with measurements; that is, we

ignore those elements not measured in a given star. In Figure 5a we plot $[\text{Z}/\text{H}]$ versus $[\text{Fe}/\text{H}]$, including all stars in our sample ($N = 190$). Panels (b) and (c) in Figure 5 show the MDFs for $[\text{Fe}/\text{H}]$ and $[\text{Z}/\text{H}]$, respectively, in regular and generalized histogram format. The regular histogram again uses the Shimazaki & Shinomoto (2007) optimal bin width algorithm (0.278 dex for $[\text{Z}/\text{H}]$). We note that the two MDFs exhibit a similar behavior. Indeed, the $[\text{Fe}/\text{H}]$ and $[\text{Z}/\text{H}]$ MDFs have almost identical average gradients over the plotted range. The construction of the $[\text{Z}/\text{H}]$ MDF, based on large samples of

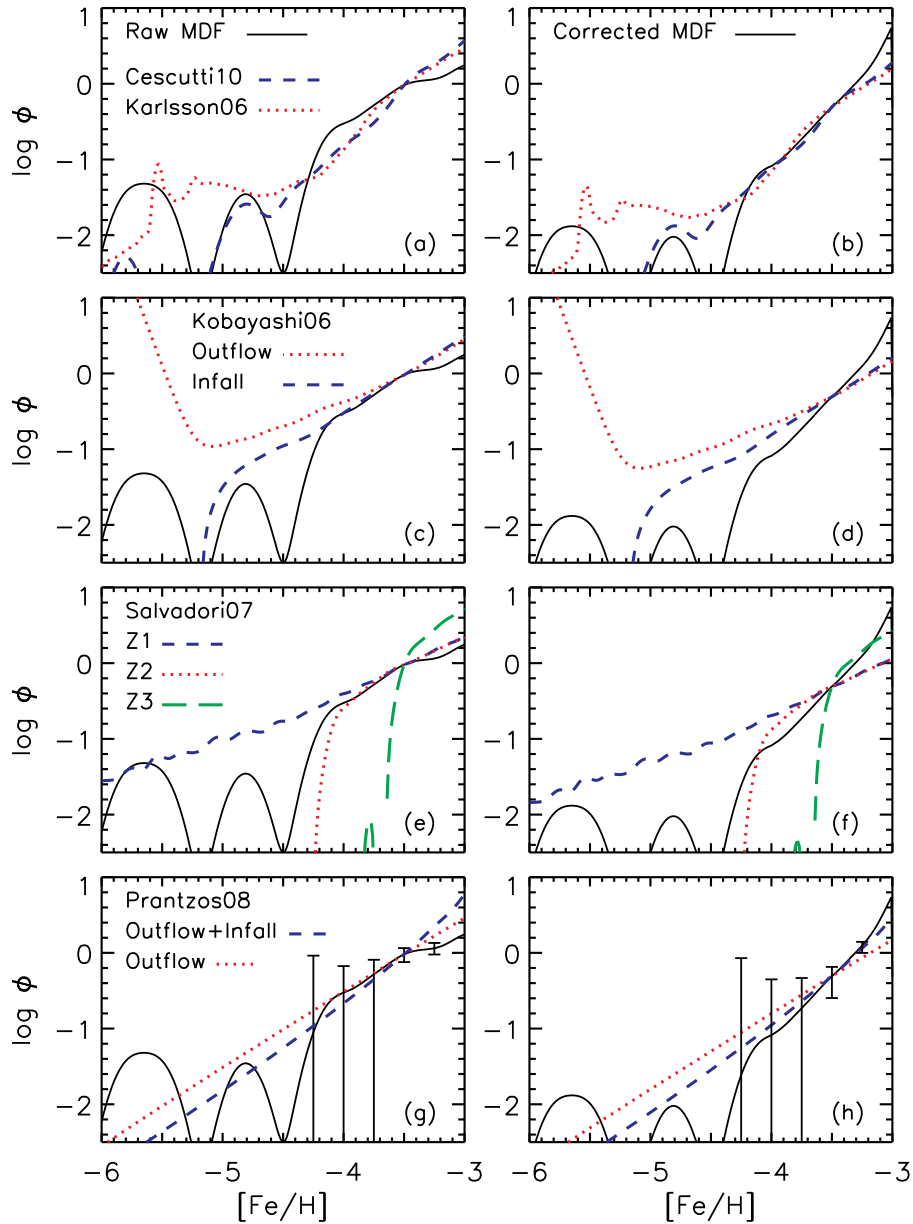


FIG. 3.— Comparison of the raw (left) and corrected (right) MDFs with the Karlsson (2006), Kobayashi et al. (2006), Salvadori et al. (2007), Prantzos (2008), and Cescutti & Chiappini (2010) predictions. The predictions are scaled to match our MDF at $[\text{Fe}/\text{H}] = -3.5$. In panels (e,f), the Z1, Z2, and Z3 lines represent critical metallicities of $Z_{\text{cr}} = 0$, $10^{-4}Z_{\odot}$, and $10^{-3.4}Z_{\odot}$ respectively. In the lower panels, we show error bars on our raw and corrected MDFs.

stars having O and C measurements, would be of great interest given the postulated importance of these elements for low-mass star formation in the early Universe (Bromm & Larson 2004; Frebel et al. 2007a). Additionally, when considering the $[\text{Z}/\text{H}]$ MDF, we need to be mindful of issues including (a) giants, in general, offer a larger suite of measurable elements than dwarfs, (b) for a fixed abundance, the lines in giants are generally stronger than in dwarfs, thereby enabling measurements in giants, rather than limits for dwarfs, in many cases, and (c) the highest values of Z in Figure 5c likely suffer from large incompleteness. Furthermore, we note that inclusion of C, N, and O abundances may considerably alter the $[\text{Z}/\text{H}]$ MDF compared to our present distribution. (We emphasize again that throughout the present paper the MDF refers to the $[\text{Fe}/\text{H}]$ distribution function unless specified otherwise.)

Armed with sufficient observational data, MDFs can of

course be constructed for a range of specific elements, e.g., $[\text{O}/\text{H}]$ and $[\text{C}/\text{H}]$, rather than just for $[\text{Fe}/\text{H}]$ or $[\text{Z}/\text{H}]$. Such element-specific MDFs can then be compared with the outputs of various chemical evolution models, as we did for $[\text{Fe}/\text{H}]$ in Figure 3. Doing so may provide valuable insights into the triumphs and deficiencies of those models, and indicate ways in which they can be improved.

3.3. The Fraction of Carbon-Enhanced Metal-Poor (CEMP) Stars

In Figure 6, we again plot the raw MDF (using generalized histograms), but on this occasion we also include in the figure the MDF when restricted to CEMP objects, where we have used the CEMP definition of Aoki et al. (2007) ($[\text{C}/\text{Fe}] \geq +0.70$, for $\log(L/L_{\odot}) \leq 2.3$ and $[\text{C}/\text{Fe}] \geq +3.0 - \log(L/L_{\odot})$, for $\log(L/L_{\odot}) > 2.3$; as opposed to the Beers & Christlieb

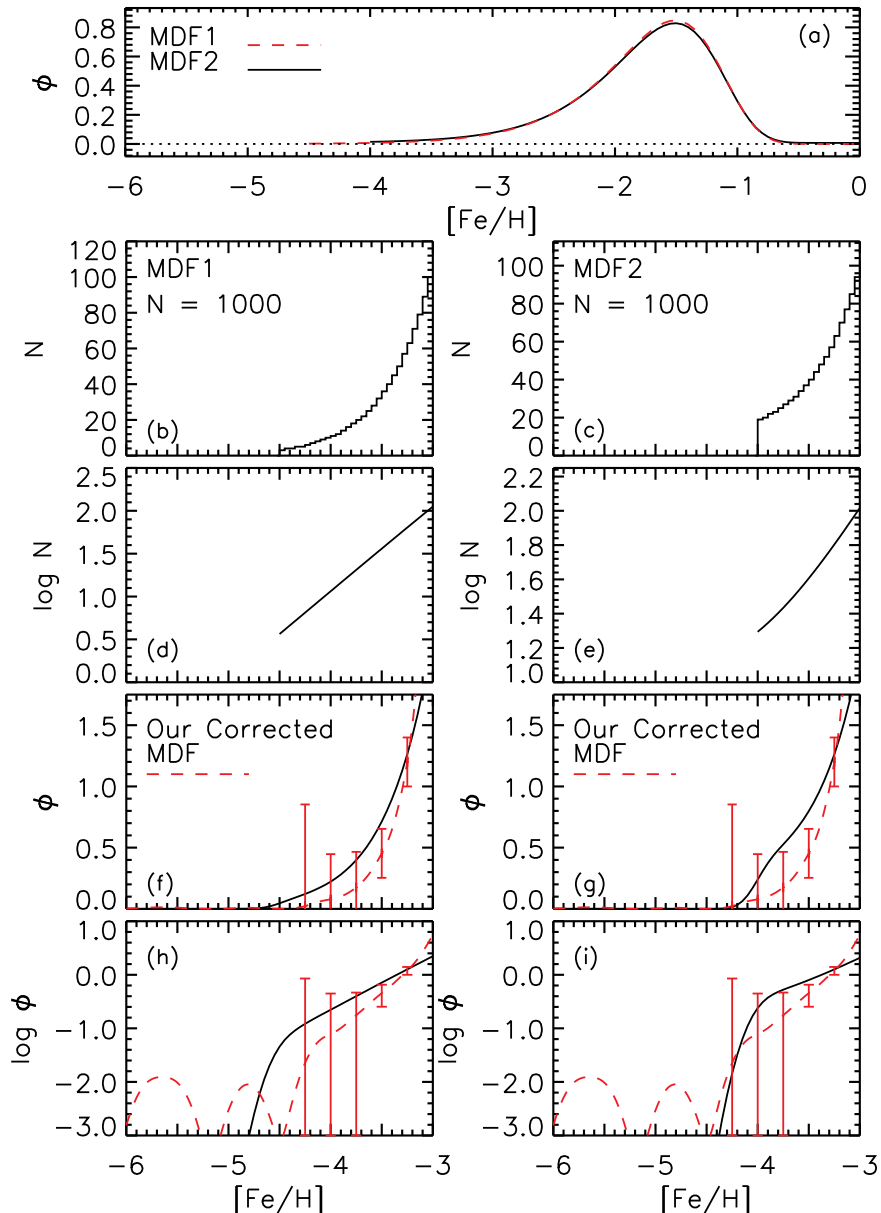


FIG. 4.— Comparison of the lower-metallicity cutoff (MDF1) and higher-metallicity cutoff (MDF2) cases generated using the Simple Model. Panels (a,b,c,f,g) are on a linear scale while panels (d,e,h,i) are on a logarithmic scale. Panels (b) through (e) are regular histograms while panels (f) through (i) are generalized histograms. Our corrected MDF is overplotted in panels (f) through (i) along with error bars. Panel (f) is normalized so the total area is 1.0, and panel (h) is produced directly from this panel. In panels (f) through (i), we overplot our corrected MDF adopting the error bars from the raw MDF (we do not show error bars below $[\text{Fe}/\text{H}] = -4.25$ since they extend beyond the range of these plots).

(2005) definition of $[\text{C}/\text{Fe}] > +1.0$). In panel (c) we show the percentage of CEMP stars as a function of $[\text{Fe}/\text{H}]$, which we obtain by dividing the CEMP MDF by the MDF containing only those stars with C-measurements or C-limits below the CEMP threshold. (Here we present results using the CEMP definitions of both Aoki et al. 2007 and Beers & Christlieb 2005.) Using Monte Carlo simulations, as described earlier, we estimate the fractional uncertainty in the CEMP MDF, and therefore the uncertainty in the CEMP percentage at a given $[\text{Fe}/\text{H}]$. Note that for our 38 program stars from Paper I, C abundances (or limits) were measured from the spectra. For the literature sample, we were unable to conduct the necessary spectrum synthesis re-analysis (since we did not have access to the spectra), and we chose not to make any adjustments to these abundances based on our adopted stellar parameters

and metallicity¹⁹. We also note that for stars with large $[\text{C}/\text{Fe}]$ ratios (and for metal-poor stars in general), a more rigorous chemical abundance analysis would require, amongst other things, model atmospheres with appropriate CNO abundances and consideration of 3D and/or non-LTE effects (Asplund 2005). Bearing in mind these shortcomings, as well as issues regarding selection biases and completeness of our sample already discussed, we now comment on the fraction of CEMP stars.

¹⁹ Had we updated the $[\text{C}/\text{Fe}]$ ratio via $[\text{C}/\text{Fe}]_{\text{New}} = [\text{C}/\text{Fe}]_{\text{Literature}} - ([\text{Fe}/\text{H}]_{\text{This study}} - [\text{Fe}/\text{H}]_{\text{Literature}})$, the numbers of CEMP objects would change from 16 to 19 and from 22 to 28 for the Beers & Christlieb (2005) and Aoki et al. (2007) definitions, respectively. However, we note that this approach only includes changes to the metallicity, and does not address any changes in the C abundance.

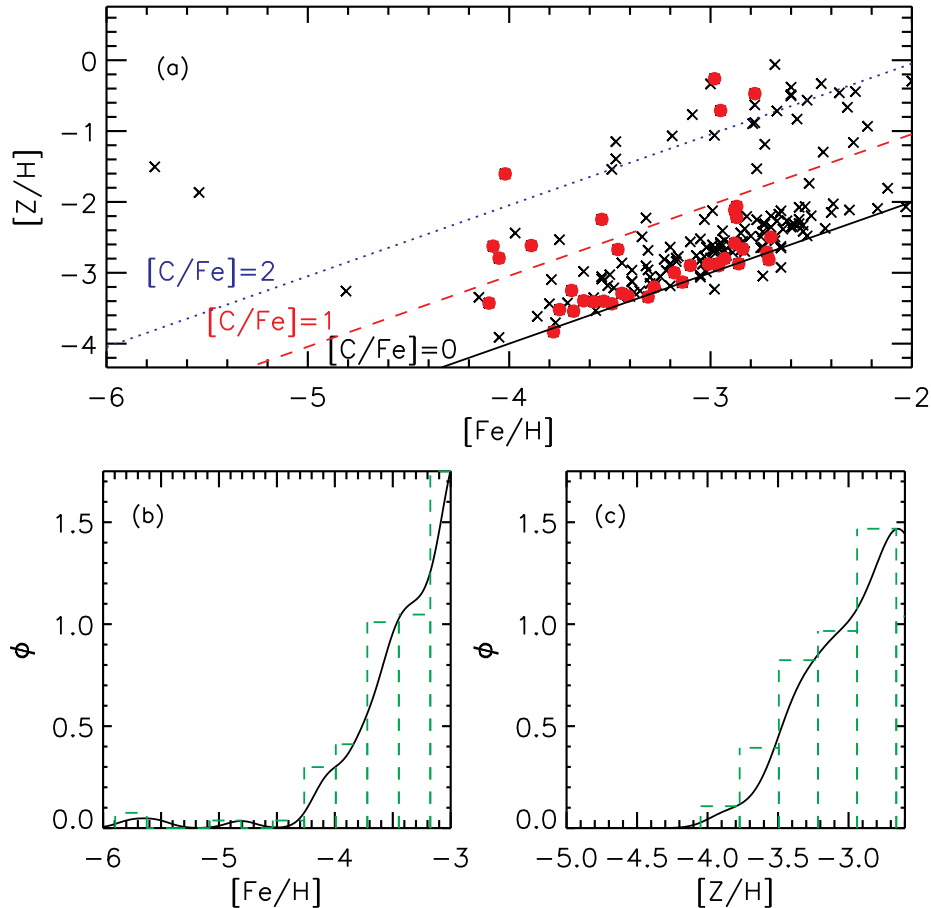


FIG. 5.— $[Z/H]$ vs. $[Fe/H]$ for the full sample of stars ($N = 190$). Program stars are plotted as red circles. Panel (a) includes lines of constant $[C/Fe]$. In panels (b) and (c), we show regular and generalized histograms for $[Fe/H]$ and $[Z/H]$, respectively, where Z includes the available set of C, N, Mg, Si, and Fe abundances in a given star.

We find a CEMP fraction of $32 \pm 8\%$ (22 of 69) adopting the Aoki et al. (2007) criteria²⁰, and $23 \pm 6\%$ (16 of 71) using the Beers & Christlieb (2005) criterion for $[Fe/H] \leq -3.0$. (As noted above, in determining the CEMP fraction we only adopt stars for which we had C measurements or C limits below the CEMP threshold. Thus, the total number of stars is not 86. Adopting the Aoki et al. (2007) criteria, we find CEMP fractions of $25 \pm 8\%$ (11 of 44) and $29 \pm 15\%$ (5 of 17) in the metallicity ranges $-3.5 < [Fe/H] \leq -3.0$ and $-4.0 < [Fe/H] \leq -3.5$, respectively. Previous estimates of the CEMP fraction below $[Fe/H] = -2.0$, using the Beers & Christlieb (2005) $[C/Fe] \geq +1.0$ criterion, include $14 \pm 4\%$ Cohen et al. (2005), $9 \pm 2\%$ Frebel et al. (2006), and $21 \pm 2\%$ Lucatello et al. (2006), all of which are probably comparable with our value, given the differences in $[Fe/H]$ ranges for the samples. For the 38 program stars of Paper I, there was a bias towards CEMP objects. Our somewhat subjective observing criteria at the Keck and Magellan telescopes, as applied to an evolving candidate list, was to (i) observe the most metal-poor candidates available, (ii) in the event of similar metallicity estimates, prefer giants over dwarfs, and (iii) for more metal-rich candidates, observe objects with prominent G -bands in their medium-resolution spectra, with the expectation that a small fraction might be C-rich, r -process enhanced stars sim-

ilar to CS 22892-052, some of which might have measurable Th and U for cosmo-chronometric age determinations (e.g., Barklem et al. 2005; Sneden et al. 2008).

Within our sample, the CEMP fraction is higher for dwarfs ($50 \pm 31\%$; 4 of 8) than for giants ($39 \pm 11\%$; 18 of 46). This discrepancy may reflect the fact that, for a fixed metallicity and $[C/Fe]$ abundance ratio, the CH molecular lines are stronger, and therefore more likely to yield a measurement, in giants than in dwarfs. That is, some of our dwarfs have such high $[C/Fe]$ limits that they may indeed have $[C/Fe] \geq +0.7$, and thus the CEMP fraction for dwarf stars is very likely an upper limit. Indeed, some 23 of 31 ($74 \pm 20\%$) dwarf stars have C limits (or no measurements), compared with only 9 of 55 ($16 \pm 6\%$) giant stars.

There are previous reports in the literature that the CEMP fraction rises with decreasing metallicity (see Carollo et al. 2012 for a full description). Including the Caffau et al. (2011) object, three of the four stars with $[Fe/H] \leq -4.5$ are CEMP objects. For our sample, of the 65 stars with $-4.3 \leq [Fe/H] \leq -3.0$ and $[C/Fe]$ measurements, 19 are CEMP objects. Adopting this CEMP fraction of 0.29, the probability of having three CEMP objects in a sample of four stars, as is the case for $[Fe/H] \leq -4.5$, is 0.076. While further data are clearly necessary to settle the issue, relative carbon richness at the lowest values of $[Fe/H]$ seems ubiquitous. We refer the reader to Carollo et al. (2012, and references therein), who demonstrate that the CEMP fraction increases from 0.05 to 0.26 ± 0.03

²⁰ If we had considered stars with $[Fe/H] \leq -2.80$, an arbitrarily chosen more metal-rich boundary, we would have obtained a CEMP fraction of $29 \pm 6\%$ (28 of 98), using the Aoki et al. 2007 definition.

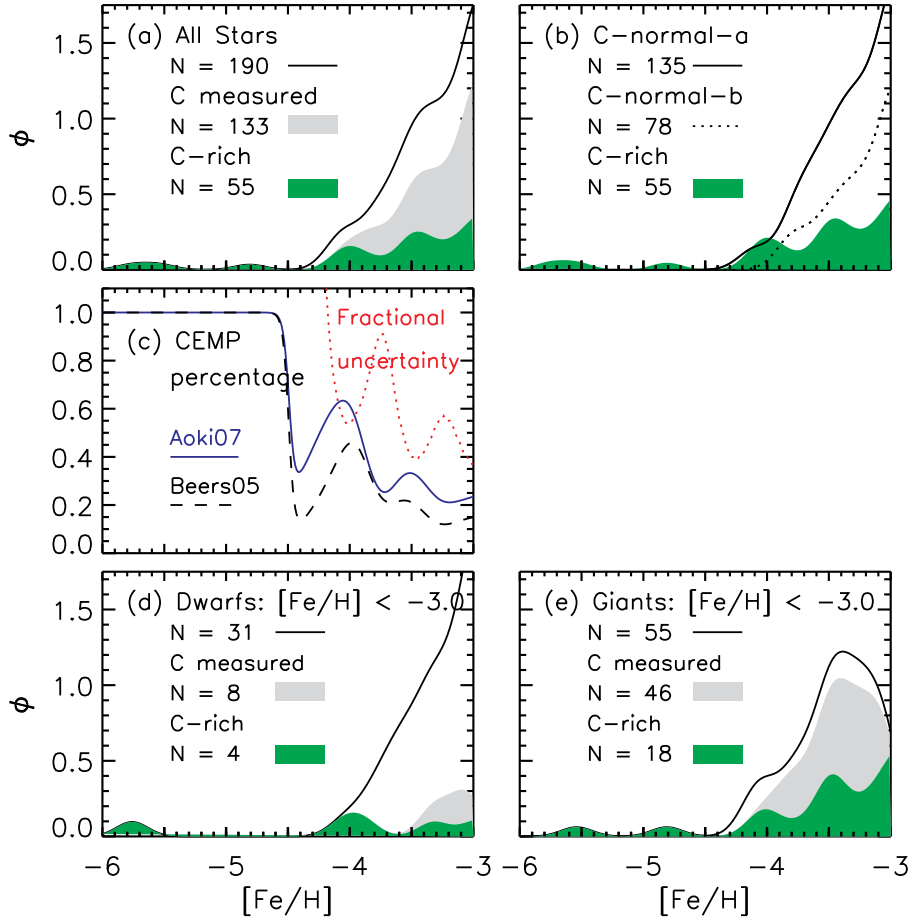


FIG. 6.— Generalized histograms showing the raw MDF for all stars (solid black line), CEMP objects (green histogram), and stars for which $[C/Fe]$ was measured (grey histogram). Panel (b) shows the MDF for (i) the C-normal population including stars with $[C/Fe]$ limits (C-normal-a), (ii) the C-normal population excluding stars with $[C/Fe]$ limits (C-normal-b), and (iii) the CEMP sample. Panel (c) shows the CEMP fraction and the fractional uncertainty. Panels (d) and (e) show dwarfs and giants, respectively.

as $[Fe/H]$ as the metallicity decreases from $[Fe/H] = -1.5$ to $[Fe/H] = -2.8$, based on a large sample of calibration stars from the Sloan Digital Sky Survey (SDSS; York et al. 2000; Gunn et al. 2006).

The above comments notwithstanding, in Figure 7 we plot the CEMP fraction as a function of $[Fe/H]$ (upper panel) and $[Z/H]$ (lower panel). For $-4.5 \leq [Fe/H] \leq -3.0$, we have three bins with roughly equal numbers, while the fourth bin, $[Fe/H] \leq -4.5$, has only 3 stars. There is no significant correlation between the CEMP fraction in each bin at the median $[Fe/H]$ of each bin; Figure 7(a) suggests a slope of -0.24 ± 0.22 . Had we included the C-normal ultra metal-poor Caffau et al. (2011) star, we would have obtained a slope of -0.20 ± 0.19 . For $[Z/H]$, we use four bins with equal numbers of stars. We again measure the linear fit to the CEMP fraction at the median $[Z/H]$ of each bin. In this case, there is no significant correlation between the CEMP fraction in each bin at the median $[Z/H]$ of each bin; Figure 7(b) suggests a slope of 0.03 ± 0.10 . An important consideration is that the sample was selected to have low metallicity such that the stars with the highest Z tend to have high C abundances. Such a bias may potentially explain the positive trend we find between CEMP fraction and $[Z/H]$. Thus, we reiterate the need to measure O and N when possible to better define the metallicity, Z . Nevertheless, we caution that the behavior of the CEMP fraction at lowest metallicity likely depends on the adopted “metallicity”

definition.

4. CONCLUDING REMARKS

We have conducted a homogeneous abundance analysis of extremely metal-poor stars from an equivalent-width analysis based on high-resolution, high-S/N spectra. Our sample contains 86 objects with $[Fe/H] \leq -3.0$, including 32 below $[Fe/H] = -3.5$. While the completeness functions for our ~ 30 HES program stars and the ~ 50 HK stars in the extended sample are well understood, the selection biases for the remaining literature sample are poorly known. Nevertheless, our results provide an important new view of the MDF and CEMP fraction at lowest metallicity.

The raw and corrected MDFs do not show evidence for a cutoff at $[Fe/H] = -3.6$. Both MDFs appear to decrease smoothly down to at least $[Fe/H] = -4.1$. Four stars with much lower metallicity are also known, three of which are present in our sample (the fourth being SDSS J102915+172927; Caffau et al. 2011).

The fraction of CEMP stars in our sample below $[Fe/H] = -3.0$ is $23 \pm 6\%$ and $32 \pm 8\%$, when adopting the Beers & Christlieb (2005) and Aoki et al. (2007) definitions, respectively. The former value is in good agreement with previous estimates (based on the Beers & Christlieb 2005 criterion). It is unclear whether the CEMP fraction increases with decreasing metallicity below $[Fe/H] = -3$, as the apparent trend is not statistically significant ($< 1\sigma$) in the present

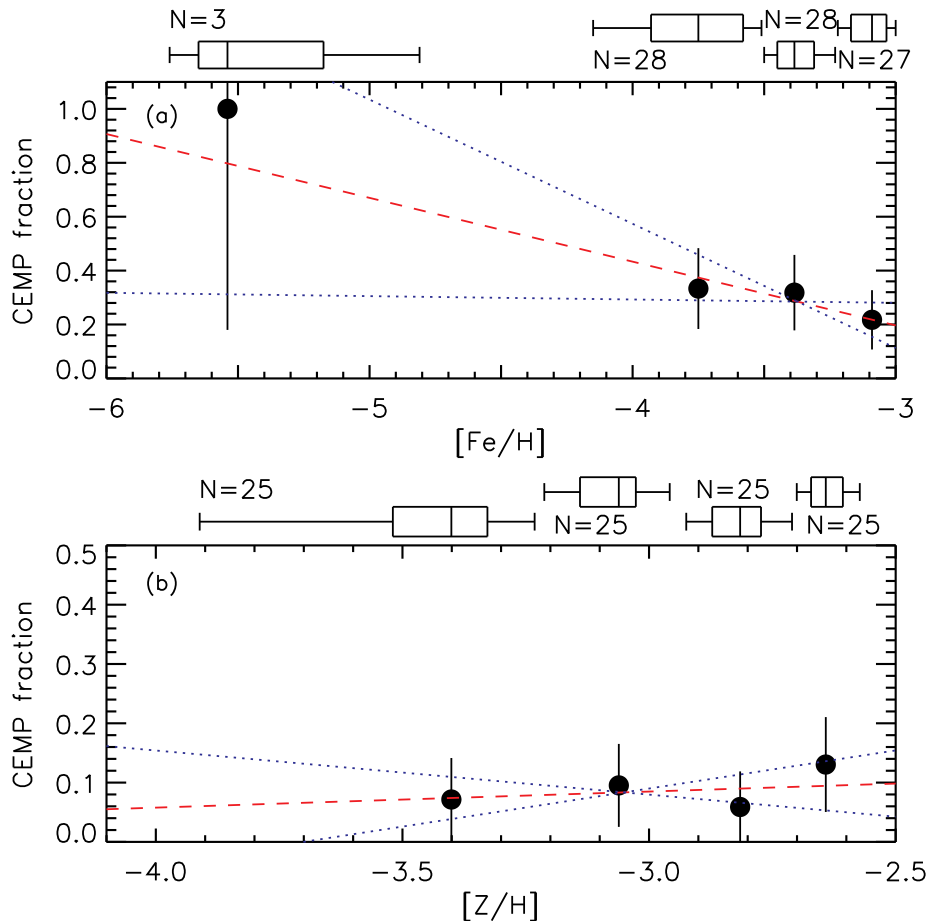


FIG. 7.— CEMP fraction versus $[\text{Fe}/\text{H}]$ (upper) and $[\text{Z}/\text{H}]$ (lower). In the upper panel, the lowest metallicity bin covers $[\text{Fe}/\text{H}] \leq -4.5$ while the three remaining metallicity bins have roughly equal numbers of stars. In the lower panel, the four metallicity bins contain equal numbers of stars. The boxplots above both panels show the distributions in metallicity and the numbers of stars per bin. In both panels, the red dashed line is the linear fit to the binned data (slope and uncertainty are given) and the blue dotted line shows the $1\text{-}\sigma$ uncertainties to the best fit.

dataset.

This study has pushed the boundary for any possible cutoff of the MDF down to at least $[\text{Fe}/\text{H}] < -4.1$, but stars below this metallicity are already known. Exploring the regime below $[\text{Fe}/\text{H}] = -4$ requires still larger samples of metal-poor stars, coupled with a more rigorous analysis that includes non-LTE effects, 3D hydrodynamical model atmospheres and, due to the prevalence of CEMP stars, appropriate CNO abundances. Upcoming surveys will hopefully produce significant numbers of metal-poor stars in the near future to address this need.

We thank C. Chiappini, T. Karlsson, C. Kobayashi, N. Prantzos, and S. Salvadori for sending electronic data, and A. Alves-Brito, A. Karakas, and R. Izzard for helpful discussions. We thank the anonymous referee for a careful reading of the paper and helpful comments. D. Y., J. E. N., M. S. B., and M. A. gratefully acknowledge support from the Australian Research Council (grants DP03042613, DP0663562, DP0984924, and FL110100012) for studies of the Galaxy's most metal-poor stars and ultra-faint satellite systems. J. E. N. and D. Y. acknowledge financial support from the Access to Major Research Facilities Program, under the International Science Linkages Program of the Australian Federal

Government. Australian access to the Magellan Telescopes was supported through the Major National Research Facilities program. Observations with the Keck Telescope were made under Gemini exchange time programs GN-2007B-C-20 and GN-2008A-C-6. N. C. acknowledges financial support for this work through the Global Networks program of Universität Heidelberg and Sonderforschungsbereich SFB 881 "The Milky Way System" (subproject A4) of the German Research Foundation (DFG). T. C. B. acknowledges partial funding of this work from grants PHY 02-16783 and PHY 08-22648: Physics Frontier Center/Joint Institute for Nuclear Astrophysics (JINA), awarded by the U.S. National Science Foundation. P. S. B. acknowledges support from the Royal Swedish Academy of Sciences and the Swedish Research Council. P. S. B. is a Royal Swedish Academy of Sciences Research Fellow supported by a grant from the Knut and Alice Wallenberg Foundation. The authors wish to recognize and acknowledge the very significant cultural role and reverence that the summit of Mauna Kea has always had within the indigenous Hawaiian community. We are most fortunate to have the opportunity to conduct observations from this mountain. Finally, we are pleased to acknowledge support from the European Southern Observatory's Director's Discretionary Time Program.

Facilities: ATT(DBS); Keck:I(HIRES); Magellan:Clay(MIKE); VLT:Kueyen(UVES)

REFERENCES

- Aoki, W. 2010, in IAU Symposium, Vol. 265, IAU Symposium, ed. K. Cunha, M. Spite, & B. Barbuy, 111
- Aoki, W., Beers, T. C., Christlieb, N., Norris, J. E., Ryan, S. G., & Tsangarides, S. 2007, *ApJ*, 655, 492
- Aoki, W., Frebel, A., Christlieb, N., Norris, J. E., Beers, T. C., Minezaki, T., Barklem, P. S., Honda, S., Takada-Hidai, M., Asplund, M., Ryan, S. G., Tsangarides, S., Eriksson, K., Steinhauer, A., Deliyannis, C. P., Nomoto, K., Fujimoto, M. Y., Ando, H., Yoshii, Y., & Kajino, T. 2006, *ApJ*, 639, 897
- Aoki, W., Norris, J. E., Ryan, S. G., Beers, T. C., & Ando, H. 2002, *PASJ*, 54, 933
- Asplund, M. 2005, *ARA&A*, 43, 481
- Asplund, M., Grevesse, N., Sauval, A. J., & Scott, P. 2009, *ARA&A*, 47, 481
- Barklem, P. S., Christlieb, N., Beers, T. C., Hill, V., Bessell, M. S., Holmberg, J., Marsteller, B., Rossi, S., Zickgraf, F., & Reimers, D. 2005, *A&A*, 439, 129
- Beers, T. C. & Christlieb, N. 2005, *ARA&A*, 43, 531
- Beers, T. C., Preston, G. W., & Shectman, S. A. 1985, *AJ*, 90, 2089
- . 1992, *AJ*, 103, 1987
- Beers, T. C., Rossi, S., Norris, J. E., Ryan, S. G., & Shefler, T. 1999, *AJ*, 117, 981
- Bonifacio, P., Molaro, P., Sivarani, T., Cayrel, R., Spite, M., Spite, F., Plez, B., Andersen, J., Barbuy, B., Beers, T. C., Depagne, E., Hill, V., François, P., Nordström, B., & Primas, F. 2007, *A&A*, 462, 851
- Bonifacio, P., Spite, M., Cayrel, R., Hill, V., Spite, F., François, P., Plez, B., Ludwig, H., Caffau, E., Molaro, P., Depagne, E., Andersen, J., Barbuy, B., Beers, T. C., Nordström, B., & Primas, F. 2009, *A&A*, 501, 519
- Bromm, V. & Larson, R. B. 2004, *ARA&A*, 42, 79
- Caffau, E., Bonifacio, P., François, P., Sbordone, L., Monaco, L., Spite, M., Spite, F., Ludwig, H.-G., Cayrel, R., Zaggia, S., Hammer, F., Randich, S., Molaro, P., & Hill, V. 2011, *Nature*, 477, 67
- Carollo, D., Beers, T. C., Bovy, J., Sivarani, T., Norris, J. E., Freeman, K. C., Aoki, W., Lee, Y. S., & Kennedy, C. R. 2012, *ApJ*, 744, 195
- Carretta, E., Gratton, R., Cohen, J. G., Beers, T. C., & Christlieb, N. 2002, *AJ*, 124, 481
- Castelli, F. & Kurucz, R. L. 2003, in IAU Symp. 210, *Modelling of Stellar Atmospheres*, ed. N. Piskunov, W. W. Weiss, & D. F. Gray (San Francisco, CA: ASP), A20
- Cayrel, R., Depagne, E., Spite, M., Hill, V., Spite, F., François, P., Plez, B., Beers, T., Primas, F., Andersen, J., Barbuy, B., Bonifacio, P., Molaro, P., & Nordström, B. 2004, *A&A*, 416, 1117
- Cescutti, G. & Chiappini, C. 2010, *A&A*, 515, 102
- Christlieb, N., Gustafsson, B., Korn, A. J., Barklem, P. S., Beers, T. C., Bessell, M. S., Karlsson, T., & Mizuno-Wiedner, M. 2004, *ApJ*, 603, 708
- Cohen, J. G., Christlieb, N., Beers, T. C., Gratton, R., & Carretta, E. 2002, *AJ*, 124, 470
- Cohen, J. G., Christlieb, N., McWilliam, A., Shectman, S., Thompson, I., Melendez, J., Wisotzki, L., & Reimers, D. 2008, *ApJ*, 672, 320
- Cohen, J. G., McWilliam, A., Shectman, S., Thompson, I., Christlieb, N., Melendez, J., Ramirez, S., Swensson, A., & Zickgraf, F. 2006, *AJ*, 132, 137
- Cohen, J. G., Shectman, S., Thompson, I., McWilliam, A., Christlieb, N., Melendez, J., Zickgraf, F., Ramirez, S., & Swenson, A. 2005, *ApJ*, 633, L109
- Frebel, A., Christlieb, N., Norris, J. E., Beers, T. C., Bessell, M. S., Rhee, J., Fechner, C., Marsteller, B., Rossi, S., Thom, C., Wisotzki, L., & Reimers, D. 2006, *ApJ*, 652, 1585
- Frebel, A., Johnson, J. L., & Bromm, V. 2007a, *MNRAS*, 380, L40
- Frebel, A. & Norris, J. E. 2011, arXiv:1102.1748
- Frebel, A., Norris, J. E., Aoki, W., Honda, S., Bessell, M. S., Takada-Hidai, M., Beers, T. C., & Christlieb, N. 2007b, *ApJ*, 658, 534
- Gunn, J. E., Siegmund, W. A., Mannery, E. J., et al. 2006, *AJ*, 131, 2332
- Hartwick, F. D. A. 1976, *ApJ*, 209, 418
- Honda, S., Aoki, W., Ando, H., Izumiura, H., Kajino, T., Kambe, E., Kawanomoto, S., Noguchi, K., Okita, K., Sadakane, K., Sato, B., Takada-Hidai, M., Takeda, Y., Watanabe, E., Beers, T. C., Norris, J. E., & Ryan, S. G. 2004, *ApJS*, 152, 113
- Izzard, R. G., Glebbeek, E., Stancliffe, R. J., & Pols, O. R. 2009, *A&A*, 508, 1359
- Karlsson, T. 2006, *ApJ*, 641, L41
- Kobayashi, C., Umeda, H., Nomoto, K., Tominaga, N., & Ohkubo, T. 2006, *ApJ*, 653, 1145
- Komiya, Y., Suda, T., Minaguchi, H., Shigeyama, T., Aoki, W., & Fujimoto, M. Y. 2007, *ApJ*, 658, 367
- Lai, D. K., Bolte, M., Johnson, J. A., Lucatello, S., Heger, A., & Woosley, S. E. 2008, *ApJ*, 681, 1524
- Laird, J. B., Carney, B. W., Rupen, M. P., & Latham, D. W. 1988, *AJ*, 96, 1908
- Li, H. N., Christlieb, N., Schörck, T., Norris, J. E., Bessell, M. S., Yong, D., Beers, T. C., Lee, Y. S., Frebel, A., & Zhao, G. 2010, *A&A*, 521, A10
- Lucatello, S., Beers, T. C., Christlieb, N., Barklem, P. S., Rossi, S., Marsteller, B., Sivarani, T., & Lee, Y. S. 2006, *ApJ*, 652, L37
- Lucatello, S., Gratton, R. G., Beers, T. C., & Carretta, E. 2005, *ApJ*, 625, 833
- Norris, J. E. 1999, in *Astronomical Society of the Pacific Conference Series*, Vol. 165, *The Third Stromlo Symposium: The Galactic Halo*, ed. B. K. Gibson, R. S. Axelrod, & M. E. Putman, 213
- Norris, J. E., Christlieb, N., Korn, A. J., Eriksson, K., Bessell, M. S., Beers, T. C., Wisotzki, L., & Reimers, D. 2007, *ApJ*, 670, 774
- Norris, J. E., Ryan, S. G., & Beers, T. C. 2001, *ApJ*, 561, 1034
- Pagel, B. E. J. & Patchett, B. E. 1975, *MNRAS*, 172, 13
- Prantzos, N. 2008, *A&A*, 489, 525
- Ryan, S. G. & Norris, J. E. 1991, *AJ*, 101, 1865
- Salvadori, S., Schneider, R., & Ferrara, A. 2007, *MNRAS*, 381, 647
- Schmidt, M. 1963, *ApJ*, 137, 758
- Schörck, T., Christlieb, N., Cohen, J. G., Beers, T. C., Shectman, S., Thompson, I., McWilliam, A., Bessell, M. S., Norris, J. E., Meléndez, J., Ramírez, S., Haynes, D., Cass, P., Hartley, M., Russell, K., Watson, F., Zickgraf, F., Behnke, B., Fechner, C., Fuhrmeister, B., Barklem, P. S., Edvardsson, B., Frebel, A., Wisotzki, L., & Reimers, D. 2009, *A&A*, 507, 817
- Searle, L. & Sargent, W. L. W. 1972, *ApJ*, 173, 25
- Shimazaki, H. & Shinomoto, S. 2007, *Neural Computation*, 19, 1503
- Siegel, S. 1956, *Nonparametric statistics for the behavioral sciences* (Tokyo: McGraw-Hill Kogakusku)
- Skrutskie, M. F., Cutri, R. M., Stiening, R., Weinberg, M. D., Schneider, S., Carpenter, J. M., Beichman, C., Capps, R., Chester, T., Elias, J., Huchra, J., Liebert, J., Lonsdale, C., Monet, D. G., Price, S., Seitzer, P., Jarrett, T., Kirkpatrick, J. D., Gizis, J. E., Howard, E., Evans, T., Fowler, J., Fullmer, L., Hurt, R., Light, R., Kopan, E. L., Marsh, K. A., McCallon, H. L., Tam, R., Van Dyk, S., & Wheelock, S. 2006, *AJ*, 131, 1163
- Snedden, C. 1973, *ApJ*, 184, 839
- Snedden, C., Cowan, J. J., & Gallino, R. 2008, *ARA&A*, 46, 241
- Sobeck, J. S., Kraft, R. P., Sneden, C., Preston, G. W., Cowan, J. J., Smith, G. H., Thompson, I. B., Shectman, S. A., & Burley, G. S. 2011, *AJ*, 141, 175
- Spite, M., Cayrel, R., Plez, B., Hill, V., Spite, F., Depagne, E., François, P., Bonifacio, P., Barbuy, B., Beers, T., Andersen, J., Molaro, P., Nordström, B., & Primas, F. 2005, *A&A*, 430, 655
- Suda, T., Katsuta, Y., Yamada, S., Suwa, T., Ishizuka, C., Komiya, Y., Sorai, K., Aikawa, M., & Fujimoto, M. Y. 2008, *PASJ*, 60, 1159
- Wisotzki, L., Koehler, T., Groote, D., & Reimers, D. 1996, *A&AS*, 115, 227
- York, D. G., Adelman, J., Anderson, J. E., Jr., et al. 2000, *AJ*, 120, 1579